Tailoring of embedded dielectric alumina film in AlGaAs epilayer by selective thermal oxidation

GIULIO TAVANI,[1] ANDREA CHIAPPINI,[2] ALEXEY FEDOROV,[3] FRANCESCO SCOTOGNELLA,[4] STEFANO SANGUINETTI,[3,5] DANIEL CHRASTINA,[1] AND MONICA BOLLANI[3,*]

[1]*L-NESS, Physics Department, via Anzani 42, 22100 Como, Italy*
[2]*Institute of Photonic and Nanotechnology - Consiglio Nazionale delle Ricerche, CSMFO Lab. and FBK Photonics Unit, Povo, Italy*
[3]*Institute of Photonic and Nanotechnology - Consiglio Nazionale delle Ricerche, L-NESS, Como, Italy*
[4]*Physics Department, Politecnico di Milano, Piazza Leonardo da Vinci 32, Milano, Italy*
[5]*L-NESS and Department of Materials Science, University of Milano-Bicocca, Milano, Italy*
[*]*monica.bollani@ifn.cnr.it*

Abstract: Vertical optical confinement is a critical requirement for a wide range of III-V photonic devices where Al_2O_3 material is the typical oxide used due to its low refractive index. This oxide layer can be formed from the oxidation of AlAs in an epitaxial GaAs/AlAs/GaAs or AlGaAs/AlAs/GaAs stack, with the advantage that the top layer remains single-crystalline. The thick film oxidation of AlAs is required for photonic applications. In this article, we report the oxidation processes developed to fully convert AlAs to AlO_x films by analyzing both thin (100 nm) and thick (500 nm) AlAs films on GaAs (001) and 2° miscut GaAs (111)A substrate. Systematic microscopic characterization is performed to demonstrate the absence of any delamination at the oxide interfaces and the evolution of the diffusive oxidation process microscopically characterized is compared with an optical (μ-Raman) characterization. We demonstrate the selectivity of the AlAs oxidation process with respect to the active $Al_{0.18}Ga_{0.82}As$ layer and the GaAs substrate. Finally, the proposed method is adopted to create a high refractive index contrast between the active optical material and the environment in the specific case of a III-V photonic crystal device, highlighting the potential of this approach for non-linear photonic applications.

1. Introduction

Photonic crystals (PhC) and metasurfaces are causing a paradigm shift in nonlinear optics [1–5]. Indeed, they may become the long-sought breakthrough in the quest for miniaturized, robust, and efficient nonlinear photonic devices [4–6]. In literature, both second and third harmonic efficiencies have been shown by engineering the photonic crystal band structure and by introducing a resonance at the first harmonic wavelength. Recently, double resonant photonic crystals have been demonstrated in which both the fundamental and the second harmonic frequencies are resonant and thus spatially and temporally confined [7].

To gain efficiency, it is critical to opt for a PhC material with a relatively high second order susceptibility χ^2. Group IV semiconductors are ruled out since they are centrosymmetric, whereas one of the most promising materials for the telecommunication range is $Al_{0.18}Ga_{0.82}As$ [8]. Working with a pump source at 1550 nm, this alloy offers the highest refractive indices both at the first and the second harmonic, while AlGaAs with lower Al concentration would absorb light in the second harmonic wavelength range.

Yet, the implementation of such photonic crystal systems remains hampered by the difficulties in controlling the fabrication process. A critical demand stems from the requirement for a high index contrast between the layer and the environment to establish vertical optical confinement in the PhC. In this work an AlAs film has been epitaxially deposited on a GaAs substrate and

capped by an $Al_{0.18}Ga_{0.82}As$ active layer. The AlAs layer was then thermally oxidized into AlO_x. This should result in optical confinement in the active because of the refractive index contrast between $Al_{0.18}Ga_{0.82}As$ (n≈3.3) and AlOx (n≈1.6). Commonly, a high quality Al_2O_3 layer can be deposited through atomic layer deposition (ALD), but often this technique is not available and it is quite expensive, hence the conversion of AlAs into AlO_x is a suitable alternative. AlAs oxidation has been extensively studied for thin material layers, of the order of 100 nm, since it was fundamental to create both electrical and optical confinement in VCSELs [9,10], but not many data are present in literature on thick AlAs layers [11]. Due to the difference in lattice parameters between AlAs and AlO_x the accumulated stress during the oxidation might lead to delamination between the top layer and the oxide. Specifically, AlAs has a lattice parameter equals to 0.566 nm whereas the $Al_{0.18}Ga_{0.82}As$ lattice parameter is slightly larger than 0.565 nm. Regarding AlO_x, despite being in an amorphous phase, it has been simulated as an isotropic cubic material with a lattice parameter of 0.526 nm in literature [12]. For this reason, although thin AlAs layer oxidation is a known process [8,9,13–15], to date only few papers have reported thick AlAs oxidations in real optical devices and most of them do not delve into the process' details [16–19]. This limits the possible applications of such thick oxidized layers to create vertical optical confinement in photonic devices for linear and non-linear optical applications. Considering the delamination another possible cause suggested by Ashby et al. [20] is the sublimation of trapped As_2O_3 during the thermal treatment.

   The aim of this paper is to obtain and characterize high-quality Al-based oxides starting both from thin (100 nm) and thick (500 nm) epitaxial AlAs layers, the latter both grown on a (001) and (111) GaAs substrate. Additionally, results of a combination of microscopic and spectroscopic characterizations are shown, which demonstrate that we have selectively controlled the AlAs oxidation process preserving the AlGaAs active layer. In the last part of the paper, to validate the process at the nanoscale, this method is adopted in the specific case of a $Al_{0.18}Ga_{0.82}As$ photonic crystal grown on an AlAs layer, proving the potential of this approach for novel class of photonic devices.

2.   Experiment

To optimize the oxidation process preventing any damage or alteration of the top active layers, systems with different AlAs thicknesses have been deposited by molecular beam epitaxy (MBE) on GaAs (001) and GaAs (111) substrates, as listed in Table 1, indicated as GROWTH A, GROWTH B and GROWTH C. An X-ray diffraction (XRD) reciprocal space (224) map of the GROWTH B wafer is presented in Fig. 1(a).

Table 1. GROWTH A, GROWTH B and GROWTH C samples' structure.

Epitaxial growth	"GROWTH A"	"GROWTH B"	"GROWTH C"
Active layer	250 nm GaAs	115 nm $Al_{0.18}Ga_{0.82}As$	115 nm $Al_{0.18}Ga_{0.82}As$
BOX	100 nm AlAs	500 nm AlAs	500 nm AlAs
Substrate	GaAs (001)	GaAs (001)	GaAs (111)A

   Specifically, all GROWTH A samples are a stack of 250 nm GaAs layer on the top, a 100 nm AlAs layer in the middle and a (001) GaAs substrate [21]. In the case of GROWTH B, a 500 nm AlAs layer is embedded between a 115 nm $Al_{0.18}Ga_{0.82}As$ layer and (001) GaAs substrate. Finally in GROWTH C, the layers are identical to the GROWTH B ones, but they are epitaxially grown on a 2° miscut (111)A GaAs substrate. Both (001) and (111) substrates have been investigated since non-linear effects in photonic crystals depend on the crystal orientation [22]. All the growths were performed at 600°C with an As flux corresponding to beam equivalent pressure 1.5×10-5 torr. The growth rate was 0.5 µm/hour. To examine the oxidation process in
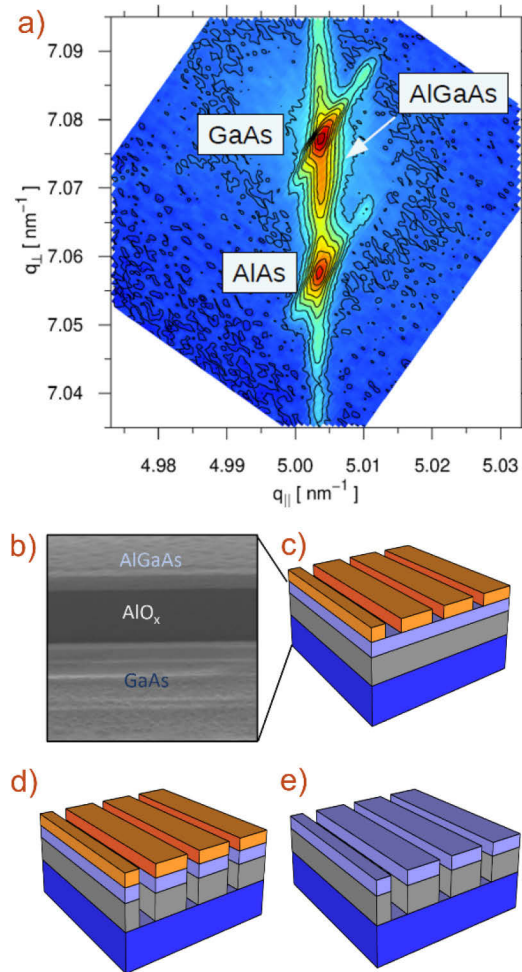
Fig. 1. XRD reciprocal space (224) map for a GROWTH B sample (1.a). In Fig. 1(c), a generic sample covered by exposed and developed resist, then the wet etching process defines the mesa down to the substrate (1.d). Finally, the resist is removed and the sample is ready to be oxidized (1.e). In Fig. 1(b), a SEM cross view of a GROWTH B sample after the oxidation, where AlGaAs thickness is 115 nm while the AlOx around 500 nm, epitaxially growth on (001) GaAs substrate.

the presented systems, rectangular mesas with different sizes have been realized: 7 μm × 200 μm, 20 μm × 200 μm, 40 μm × 200 μm and 80 μm × 200 μm. These structures were fabricated with a combination of optical lithography and selective wet etching as reported in Fig. 2. The wet etching process was carried out using a H_3PO_4:H_2O_2:H_2O solution (8:2.5:1 in volume) at room temperature for 5 to 10 seconds to define mesas down to the GaAs substrate. AlAs oxidation was then performed in a furnace with water vapor flow and N_2 as gas carrier [13–14]. The furnace temperature was set at 350 ° C (± 10 ° C) whilst the water was heated to 90 °C.
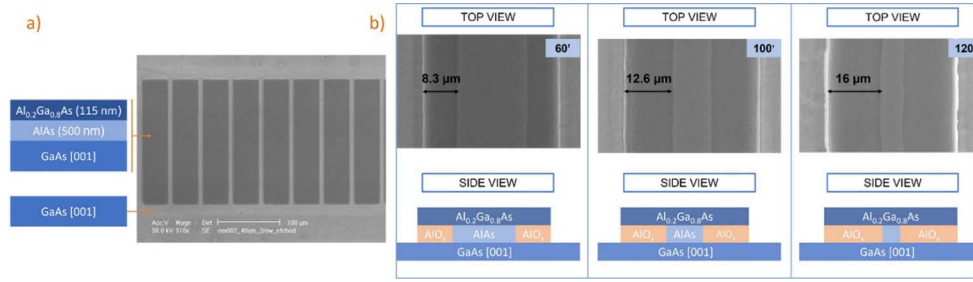
Fig. 2. On the right of Fig. 2(a), a planar view of several mesa structures after being etched and before the oxidation. On the left, a schematic side view of the patterned structures. In Fig. 2(b), planar and side views of a single mesa structure after being oxidized for 60, 100 and 120 minutes. Two lateral stripes whose extent grows in time are clearly observable. This is due to the AlO_x formation beneath the top layer.

3. Results and discussion

Several models have been proposed to describe the formation of AlO_x in time [23–26]. Deal and Grove present a simple model of thermal silicon oxidation which can be adopted for AlAs oxidation [26]. According to this, here we consider that the oxide extent (d_{ox}) evolves in time based on:

$$d_{ox}^2 + Ad_{ox} = Bt \qquad (1)$$

where B is the coefficient that describes the diffusion of reactants inside the already formed AlO_x, while the ratio B/A takes into account the oxidation rate at the interface between AlO_x and AlAs.

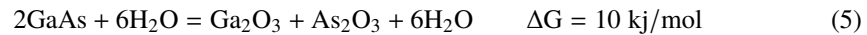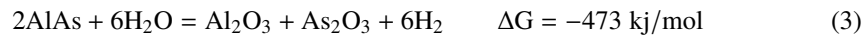For short times, d_{ox} shows a linear behavior and the Eq. (1) becomes:

$$d_{ox} = \frac{B}{A}t \qquad (2)$$

So, at first, the oxidation is limited by the reaction of the chemical species at the $AlAs/AlO_x$ interface and not by the water vapor diffusion through the oxide. As from the data reported below, this is the linear regime that characterizes our oxidative process.

For longer times, indeed, the reaction regime is different: the water vapor supply is the limiting factor, and a parabolic growth of the oxide will be observed.

Both the oxidation coefficients depend exponentially on temperature according to the Arrhenius relationship.

From physical-chemical perspective, the redox reactions are described by the following equations (3) (4) (5):

$$2AlAs + 6H_2O = Al_2O_3 + As_2O_3 + 6H_2 \qquad \Delta G = -473 \text{ kj/mol} \qquad (3)$$

$$As_2O_3 + 3H_2 = 2As + 3H_2O \qquad \Delta G = -131 \text{ kj/mol} \qquad (4)$$

$$2GaAs + 6H_2O = Ga_2O_3 + As_2O_3 + 6H_2O \qquad \Delta G = 10 \text{ kj/mol} \qquad (5)$$

where ΔG is the Gibbs free energy of the process [14]. At constant temperature and pression, a negative ΔG implies a spontaneous reaction whereas a non-spontaneous reaction would present a positive ΔG. In the series GROWTH A, the top layer is made of GaAs which is not going to oxidize since the reaction is non-spontaneous, as apparent by the Eq. (5).

In the case of GROWTH B and GROWTH C, the top layers have an Al concentration of only 20% and, since the $Al_xGa_{(1-x)}As$ oxidation rate strongly depends on the Al content, their oxidation is negligible [15]. Concerning AlAs, both As and Al are oxidized. As_2O_3 reacts with H_2 and becomes As (Eq. (4)). In the end, both As_2O_3 and pure As sublimate.

To check the residual chemical species after the oxidation, a GROWTH B sample was heated up to 500°C in a vacuum chamber after the oxidation. The chamber atmosphere was analyzed via mass spectrometry and no specific signals, including As_2O_3 and pure As, were detected. Specifically, the atomic mass of pure As is equal to 75 a.m.u. whereas the one associated to Arsenic monoxide is 91 a.m.u. Furthermore, around 75 a.m.u. is located the range related to Arsine and its dissociation products (AsH_3, AsH_2, AsH). The spectra of GROWTH B's samples recorded at room temperature, then at 350°C and finally at 500°C, show similar residual chemical species and no signal neither around 75 a.m.u. nor around 91 a.m.u. are detected (see Supplement 1 for the spectra).

Regarding Al, it has been suggested in literature that the resulting AlOx is in an amorphous hydrate phase such as $Al(OH)_3$ or AlO(OH) [13–14,27] and at 400 °C, it dehydrates to form amorphous Al_2O_3 [28].

All the samples have been fully characterized by scanning electron microscopy (SEM) before and after the various oxidation treatments at different annealing times. Compared to other characterization techniques, SEM analysis is fast and not destructive, and it is an ordinary tool present in many laboratories. Since SEM imaging is based on both secondary and backscattered electrons, a slight variation in chemical species results in a different optical contrast.

In Fig. 2(a), a SEM image of the patterned structures on a GROWTH B sample is reported. The same mesas are characterized after 60, 90 and 120 minutes of thermal treatment at 350°C (Fig. 2(b)). The observed contrast across a patterned structure is ascribed to the formation of AlO_x at the borders of the mesa while AlAs remains in the central part of the structure. Similar contrast is reported for all mesas fabricated on GROWTH A and GROWTH C samples (not shown). Observing the evolution of the contrast in time, the oxidation rates have been inferred. In this way, through a non-invasive technique, it is possible to control the selective oxidation process of AlAs with respect to an alloy of AlGaAs, on samples of varying sizes. The absence of delamination confirms the rapid desorption of As_2O_3 during annealing process, preventing stress and consequently delamination on top AlGaAs layer.

At 350 °C, which corresponds to the optimal temperature to avoid any delamination processes, the oxidation rate is equal to 7.3 μm/hour for GROWTH A, 8.3 μm/hour for the GROWTH B, and 11.2 μm/hour for GROWTH C. Regardless of the AlAs film thickness, the oxidation rates were constant in the considered time range. Hence, oxidation proceeds in the reaction limited regime, as descripted by Eq. (2) .

A systematic μ-Raman characterization followed each step of the oxidation process. The adopted instrumentation (Labram Aramis Jobin Yvon Horiba) relies on a 3 μm spot diameter which allows the oxidized borders to be distinguished from the center of the mesa. The importance of this characterization is two-fold. Firstly, it allows the results obtained with SEM imaging to be validated; secondly, it confirms that the oxidation process is selective for AlAs, leaving unaltered the AlGaAs or GaAs films deposited on top.

In Fig. 3, a μ-Raman spectrum for a GROWTH B sample is reported and the main peaks are la-belled. AlAs peaks are located at 402 cm^{-1} (LO) and at 360 cm^{-1} (TO). GaAs peaks are located at 292 cm^{-1} (LO) and 269 cm^{-1} (TO). The LO peak positions of $Al_{0.18}Ga_{0.82}As$ have been calculated using the following relations [29]:

$$\omega_{LO}^{GaAs} = 290.2 - 36.7x \ cm^{-1} \tag{6}$$

$$\omega_{LO}^{AlAs} = 364.7 + 46.7x - 9.4x^2 \ cm^{-1} \tag{7}$$

Considering x = 0.18 ω_{LO}^{GaAs} = 282 cm_{-1} and ω_{LO}^{AlAs} = 373 cm_{-1} are obtained.

The orange curve was acquired at a mesa border, whereas the blue curve was acquired at the mesa center. As SEM contrast suggests, the AlAs peaks vanish on the orange curve confirming the removal of AlAs and the AlOx formation in the darker regions as shown in the inset.
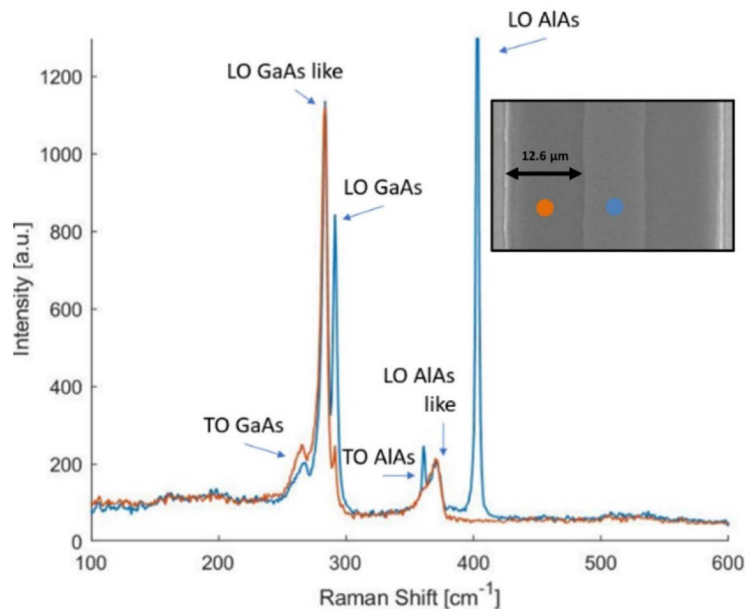
Fig. 3. Raman spectra acquired in a back-scattering configuration using a 532 nm laser for a GROWTH B sample after the oxidation process. The orange curve is obtained focusing on a the darker lateral region of the mesa whilst the blue one at the center of it. Both LO and TO AlAs peaks are no longer pre-sent on the spectrum acquired on the mesa border in account of the AlOx formation.

Figure 4 displays µ-Raman characterizations for the oxidized samples from both GROWTH A and GROWTH B series. In Fig. 4(b), LO AlAs and LO GaAs peak intensities across a GROWTH A mesa structure (line scan) are reported. The same analysis for a GROWTH B sample is shown in Fig. 4(d), showing the LO GaAs like peak related to the $Al_{0.18}Ga_{0.82}As$ top layer instead of the LO GaAs peak.

In both systems, the AlAs peaks are present only at the mesa center and drop in intensity at the border areas where AlAs is oxidized. GaAs and $Al_{0.18}Ga_{0.82}As$ peaks do not change across the structure, suggesting that the oxidation rate for the top layer is negligible, in accordance with Eq. (5).

A GROWTH C sample, based on a GaAs (111)A substrate, was also treated for 60 minutes at 350° C and characterized by both by SEM imaging and µ-Raman spectroscopy, as before. A clear contrast after the thermal process is evident in the SEM images (inset of Fig. 5) and Raman analysis (Fig. 5).

The (111) orientation is appealing in second-harmonic generation devices since it has been demonstrated that its efficiency depends on the crystal growth direction [22].

Finally, a photonic crystal (PhC) was fabricated to demonstrate that the proposed method would also be advantageous for creating a valuable low refractive index material in III-V nanophotonic devices. This result is related to the fabrication of periodic optical nanostructures to improve light-matter interaction at the nanoscale, making them useful in optical communication, sensing and spectroscopy. AlGaAs platforms, in fact, have already proved to be a crucial tool in non-linear nanophotonic, thanks to their high intrinsic second order non-linearity together with the absence of absorption of two photons at telecommunication wavelengths. Here we demonstrate the ability to realize such platforms starting from an AlGaAs / AlAs / GaAs heterostructure, adapting the oxidation process only on the AlAs layer. PhC was prepared by electron-beam lithography (EBL) upon a substrate described as "GROWTH B" cleaned by an ultrasonic treatment with organic
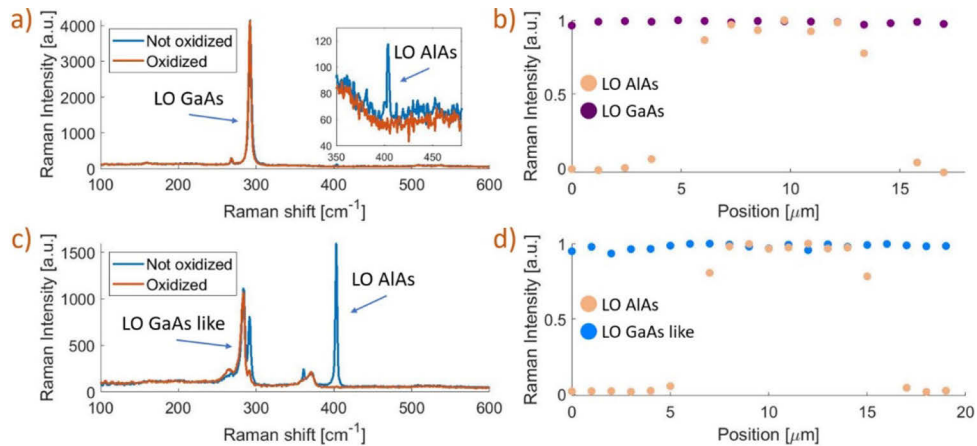
Fig. 4. (a): a spectrum acquired for a GROWTH A sample after 60 minutes of oxidation on a 20 μm X 200 μm mesa structure. In the inset, a zoom of the LO AlAs peak. (b): the evolution of the normalized intensities, after background removal, of the LO AlAs and LO GaAs peaks across the same mesa. In Fig. 4(c) and Fig. 4(d), the correspondent analysis are shown for a GROWTH B sample. In ac-count of the fact that the top layer is made of $Al_{0.18}Ga_{0.82}As$, in Fig. 4(d) the LO GaAs peak intensity is replaced by the LO GaAs like one's. The LO AlAs peak intensity difference between Fig. 4(a) and Fig. 4(c) stems from the different AlAs layer thicknesses in GROWTH A and GROWTH B samples.
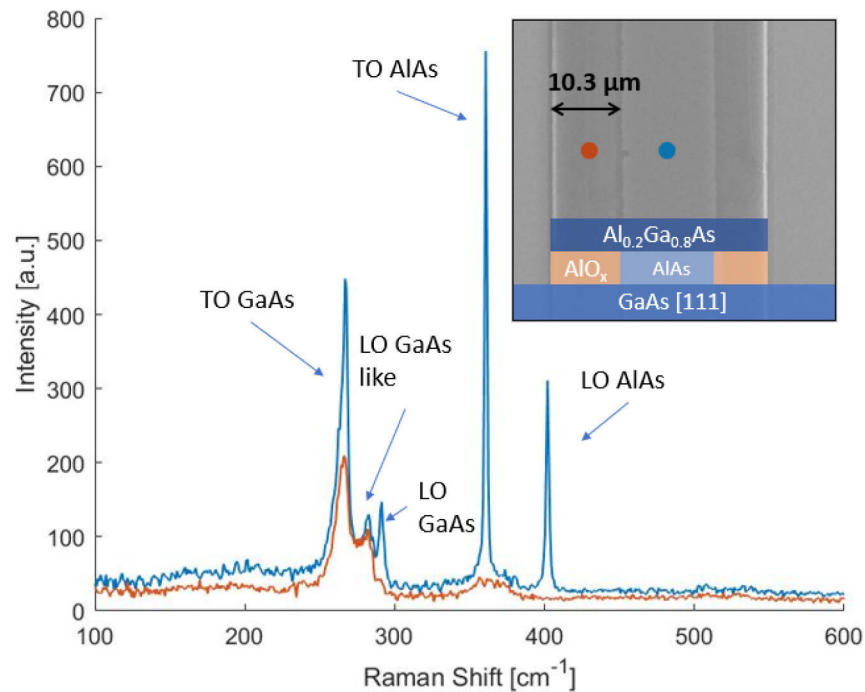

Fig. 5. Raman spectrum obtained focusing on a single mesa structure of a GROWTH C sample after the oxidation. In these spectra, TO peaks are much more intense compared to previous materials. This is due to the fact that in backscattering situation TO peaks should be theoretically forbidden for the [001] crystal orientation while they are allowed in the [111] one. In the inset, a SEM planar image of the analyzed mesa structure, superimposed the schematic cross view of the material stack after the oxidation process.

solvents such as acetone, isopropanol and N-methyl-2-pyrrolidone. During EBL, different doses were used to create holes with final radius of 180–200 nm and a hole center spacing of about 0.5 μm [30]. By wet etching of $H_3PO_4:H_2O_2:H_2O$ solution (8:2.5:1 in volume) at room temperature for 5 seconds roughly 120 nm of AlGaAs were etched. Oxidation was then performed at 350°C for 20 minutes. Water vapor diffusion was carried out through the PhC holes that were etched down to the AlAs layer.

Figure 6 shows the μ-Raman characterization of a generic PhC structure in which the defects (holes) were not tuned to a specific resonance, but it is a demonstration that our approach allows a tailoring of the oxidation process even on nanostructures.
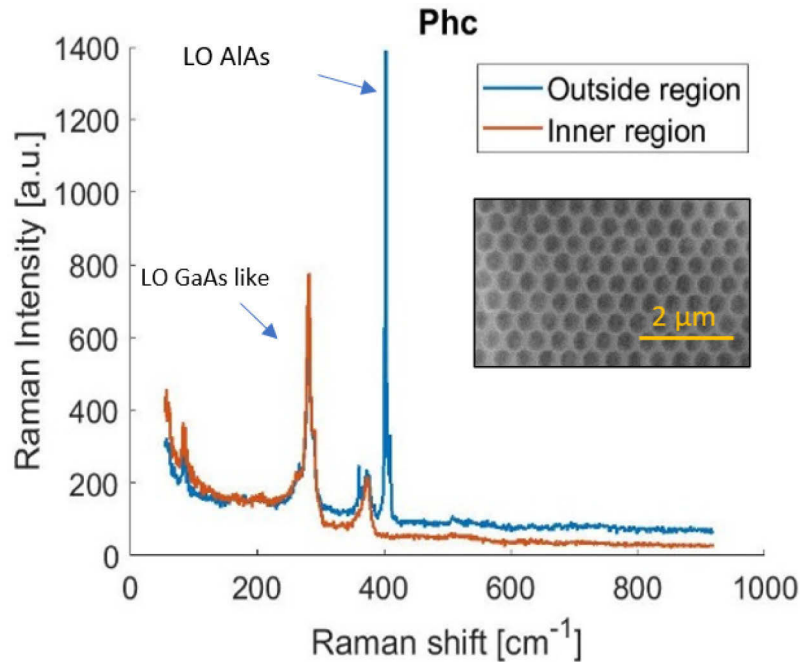

Fig. 6. Raman spectrum obtained focusing on the photonic crystal (orange curve) and in a flat area distant from the PhC (blue curve). In the inset, a zoom-in image of the photonic crystal. This has a hexagonal lattice and a hole radius of 190 nm.

A SEM characterization shows a contrast between the area close to the PhC and the area far from it; therefore μ-Raman measurements (Fig. 6) were performed focusing on these two regions. The LO AlAs peak is absent in the PhC area whereas the peak associated with the PhC layer (LO GaAs like) does not change after the oxidation.

4. Conclusion

To conclude, the selective oxidation of AlAs with respect to AlGaAs and GaAs is confirmed for a thin layer of AlAs (100 nm) and demonstrated for a thick one (500 nm). The optimal temperature for the oxidation processes is found around 350 °C: faster treatments carried out at higher temperatures (430 °C and 380 °C) led to delamination processes on the top layer. Then, we demonstrate the evolution of the diffusive oxidation process can be monitored not only by Raman spectroscopy but also by scanning electron microscopy. Compared to other characterization techniques, indeed, SEM analysis is fast and not destructive: since SEM imaging is based on both secondary and backscattered electrons, a slight variation in chemical species results in a different optical contrast. This oxidation process in relaxed films is valid not only for substrates (001) but

also for (111), demonstrating that the oxidation of AlAs does not depend on the orientation of the crystals. Finally, it has been shown that the suggested method can be exploited in a photonic device of real interest to develop new platforms for linear and non-linear photonic applications."

Disclosures. The authors declare no conflicts of interest.

Data availability. Data underlying the results presented in this paper are not publicly available at this time but may be obtained from the authors upon reasonable request.

Supplemental document. See Supplement 1 for supporting content.

References

1. A. I. Kuznetsov, A. E. Miroshnichenko, M. L. Brongersma, Y. S. Kivshar, and B. Luk'yanchuk, "Optically resonant dielectric nanostructures," Science **354**(6314), aag2472 (2016).
2. S. Liu, M. B. Sinclair, S. Saravi, G. A. Keeler, Y. Yang, J. Reno, G. M. Peake, F. Setzpfandt, I. Staude, T. Pertsch, and I. Brener, "Resonantly enhanced second-harmonic generation using iii–v semiconductor all-dielectric metasurfaces," Nano Lett. **16**(9), 5426–5432 (2016).
3. A. Krasnok, M. Tymchenko, and A. Alù, "Nonlinear metasurfaces: a paradigm shift in nonlinear optics," Mater. Today **21**(1), 8–21 (2018).
4. M. Kauranen and A. Zayats, "Nonlinear plasmonics," Nat. Photonics **6**(11), 737–748 (2012).
5. J. P. Mondia, H. M. van Driel, W. Jiang, A. R. Cowan, and J. F. Young, "Enhanced second-harmonic generation from planar photonic crystals," Opt. Lett. **28**(24), 2500–2502 (2003).
6. S. Buckley, M. Radulaski, K. Biermann, and J. Vučković, "Second harmonic generation in photonic crystal cavities in (111)-oriented GaAs," Appl. Phys. Lett. **103**(21), 211117 (2013).
7. M. Minkov, D. Gerace, and S. Fan, "Doubly resonant $\chi^{(2)}$ nonlinear photonic crystal cavity based on a bound state in the continuum," Optica **6**(8), 1039 (2019).
8. V. F. Gili, L. Carletti, A. Locatelli, D. Rocco, M. Finazzi, L. Ghirardini, I. Favero, C. Gomez, A. Lemaître, M. Celebrano, C. D. Angelis, and G. Leo, "Monolithic AlGaAs second-harmonic nanoantennas," Opt. Express **24**(14), 15965–15971 (2016).
9. M. Arai, N. Nishiyama, S. Shinada, F. Koyama, and K. Iga, "AlAs oxidation system with H_2O vaporizer for oxide-confined surface emitting lasers," Jpn. J. Appl. Phys. **39**(Part 1, No. 6A), 3468–3469 (2000).
10. S.-C. Ko, S. Lee, and Y. Chou, "Wet oxidation in a square sandwich composite of GaAs/AlAs/GaAs," J. Electron. Mater. **36**(12), 1652–1657 (2007).
11. F. Chouchane, G. Almuneau, N. Cherkashin, A. Arnoult, G. Lacoste, and C. Fontaine, "Local stress-induced effects on AlGaAs/AlOx oxidation front shape," Appl. Phys. Lett. **105**(4), 041909 (2014).
12. F. Kießling, T. Niermann, M. Lehmann, J.-H. Schulze, A. Strittmatter, A. Schliwa, and U. W. Pohl, "Strain field of a buried oxide aperture," Phys. Rev. B **91**(7), 075306 (2015).
13. K. D. Choquette, K. M. Geib, H. C. Chui, B. E. Hammons, H. Q. Hou, T. J. Drummond, and R. Hull, "Selective oxidation of buried AlGaAs versus AlAs layers," Appl. Phys. Lett. **69**(10), 1385–1387 (1996).
14. K. D. Choquette, K. M. Geib, C. I. H. Ashby, R. D. Twesten, O. Blum, H. Q. Hou, D. M. Follstaedt, B. E. Hammons, D. Mathes, and R. Hull, "Advances in selective wet oxidation of AlGaAs alloys," IEEE J. Select. Topics Quantum Electron. **3**(3), 916–926 (1997).
15. T. Langenfelder, S. Schröder, and H. Grothe, "Lateral oxidation of buried $Al_xGa_{1-x}As$ layers in a wet ambient," J. Appl. Phys. **82**(7), 3548–3551 (1997).
16. Y. Tanaka, Y. Sugimoto, N. Ikeda, T. Yang, K. Asakawa, Y. Watanabe, K. Inoue, T. Maruyama, K. Miyashita, and K. Ishida, "Fabrication and characterization of AlGaAs-based photonic crystal slab waveguides by precisely controlled self-aligned selective-oxidation process," Jpn. J. Appl. Phys. **42**(Part 1, No. 12), 7331–7338 (2003).
17. K. Welna, M. Hugues, C. P. Reardon, L. O'Faolain, M. Hopkinson, and T. F. Krauss, "Photonic crystal nanocavities in GaAs/AlGaAs with oxidised bottom cladding," Photonics and Nanostruct. - Fundamentals and Appl. **11**(2), 139–144 (2013).
18. A. M. Yacomotti, F. Raineri, G. Vecchi, I. Sagnes, M. Strassner, L. Le Gratiet, R. Raj, and A. Levenson, "Ultra-fast nonlinear response around 1.5 μm in 2D AlGaAs/AlOx photonic crystal," Appl. Phys. B **81**(2-3), 333–336 (2005).
19. E. Peter, I. Sagnes, G. Guirleo, S. Varoutsis, J. Bloch, A. Lemaître, and P. Senellart, "High-Q whispering-gallery modes in GaAs/AlOx microdisks," Appl. Phys. Lett. **86**(2), 021103 (2005).
20. C. I. H. Ashby, J. P. Sullivan, K. D. Choquette, K. M. Geib, and H. Q. Hou, "Wet oxidation of AlGaAs: the role of hydrogen," J. Appl. Phys. **82**(6), 3134–3136 (1997).
21. M. Bollani, S. Bietti, C. Frigeri, D. Chrastina, K. Reyes, P. Smereka, J. Millunchick, G. Vanacore, M. Burghammer, A. Tagliaferri, and S. Sanguinetti, "Ordered arrays of embedded Ga nanoparticles on patterned silicon substrates," Nanotechnology **25**(20), 205301 (2014).
22. S. Zanotti, M. Minkov, S. Fan, L. C. Andreani, and D. Gerace, "Doubly-resonant photonic crystal cavities for efficient second-harmonic generation in III–V semiconductors," Nanomaterials **11**(3), 605 (2021).
23. M. Ochiai, G. E. Giudice, H. Temkin, J. W. Scott, and T. M. Cockerill, "Kinetics of thermal oxidation of AlAs in water vapor," Appl. Phys. Lett. **68**(14), 1898–1900 (1996).

24. M. Osinski, T. Svimonishvili, G. A. Smolyakov, V. A. Smagley, P. Mackowiak, and W. Nakwaski, "Temperature and thickness dependence of steam oxidation of AlAs in cylindrical mesa structures," IEEE Photonics Technol. Lett. **13**(7), 687–689 (2001).

25. W. Nakwaski, M. Wasiak, P. M. kowiak, W. Bedyk, M. O. ski, A. Passaseo, V. Tasco, M. T. Todaro, M. D. Vittorio, R. Joray, J. X. Chen, R. P. Stanley, and A. Fiore, "Oxidation kinetics of AlAs and (AlGa)As layers in GaAs-based diode laser structures: comparative analysis of available experimental data," Semicond. Sci. Technol. **19**(3), 333–341 (2004).

26. B. E. Deal and A. S. Grove, "General relationship for the thermal oxidation of silicon," J. Appl. Phys. **36**(12), 3770–3778 (1965).

27. A. Blokhin, A. N. Smirnov, A. V. Sakharov, A. G. Gladyshev, N. V. Kryzhanovskaya, N. A. Maleev, A. E. Zhukov, E. S. Semenova, D. A. Bedarev, E. V. Nikitina, M. M. Kulagina, M. V. Maksimov, N. N. Ledentsov, and V. M. Ustinov, "Stresses in selectively oxidized GaAs/(AlGa)$_x$O$_y$ structures," Semiconductors **39**(7), 748–753 (2005).

28. R. Y. Li, Z. G. Wang, B. Xu, P. Jin, X. Guo, and M. Chen, "Time dependence of wet oxidized AlGaAs/GaAs distributed Bragg reflectors," J. Vac. Sci. Technol., B: Microelectron. Process. Phenom. **23**(5), 2137–2140 (2005).

29. Z. R. Wasilewski, M. M. Dion, D. J. Lockwood, P. Poole, R. W. Streater, and A. J. SpringThorpe, "Composition of AlGaAs," J. Appl. Phys. **81**(4), 1683–1694 (1997).

30. M. Bollani, D. Chrastina, A. Fedorov, R. Sordan, A. Picco, and E. Bonera, "Ge-rich islands grown on patterned Si substrates by low-energy plasma-enhanced chemical vapour deposition," Nanotechnology **21**(47), 475302 (2010).